Dynamic Shape Estimation of Tendon-Driven Soft Manipulators via Actuation Readings

Feliu-Talegon, Daniel; Mathew, Anup Teejo; Alkayas, Abdulaziz Y.; Adamu, Yusuf Abdullahi; Renda, Federico

Important note
To cite this publication, please use the final published version (if applicable).
Please check the document version above.

Dynamic Shape Estimation of Tendon-Driven Soft Manipulators via Actuation Readings

Daniel Feliu-Talegon [ORCID], *Member, IEEE*, Anup Teejo Mathew [ORCID], *Member, IEEE*, Abdulaziz Y. Alkayas [ORCID], Yusuf Abdullahi Adamu [ORCID], and Federico Renda [ORCID], *Member, IEEE*

Abstract—Soft robotic systems pose a significant challenge for traditional modeling, estimation, and control approaches, primarily owing to their inherent complexity and virtually infinite degrees of freedom (DoFs). This work introduces an innovative method for dynamically estimating the states of tendon-actuated soft manipulators. Our technique merges the Geometric Variable-Strain (GVS) approach with a kinematic formula that links the length variation of tendons to the deformations of the manipulator and a nonlinear observer design based on state-dependent Riccati equation (SDRE). In our methodology, the soft links are represented by Cosserat rods, and the robot's geometry is parameterized by the strain field along its length. Consequently, its infinite dimensions can be described by utilizing multiple degrees of freedom, depending on the required precision. This enables us to estimate the states (pose and velocity) of tendon-actuated soft manipulators solely based on tendon displacements and actuator forces. Through simulation, we demonstrate the convergence of our estimation method across various DoFs and actuator numbers, revealing a trade-off between the number of DoFs and required actuators for observing system states. Furthermore, we validate our approach with an experimental prototype of 25 cm in length, achieving an average tip position error during dynamic motion of 1.79 cm —less than 7% of the overall body length.

Index Terms—Dynamic estimation, soft robots, tendon-driven, actuation readings.

I. INTRODUCTION

INTEREST in soft robotics arises from the urgent necessity to develop robotic systems capable of seamlessly adapting

Daniel Feliu-Talegon is with the Department of Mechanical and Nuclear Engineering, Khalifa University of Science and Technology, Abu Dhabi 127788, UAE, and also with the Cognitive Robotics Department, Delft University of Technology, 2628 Delft, The Netherlands (e-mail: d.feliutalegon@tudelft.nl).

Anup Teejo Mathew and Federico Renda are with the Department of Mechanical and Nuclear Engineering, Khalifa University of Science and Technology, Abu Dhabi 127788, UAE, and also with the Khalifa University Center for Autonomous Robotic Systems (KUCARS), Khalifa University of Science and Technology, Abu Dhabi 127788, UAE (e-mail: anup.mathew@ku.ac.ae; federico.renda@ku.ac.ae).

Abdulaziz Y. Alkayas and Yusuf Abdullahi Adamu are with the Department of Mechanical and Nuclear Engineering, Khalifa University of Science and Technology, Abu Dhabi 127788, UAE (e-mail: 100052628@ku.ac.ae; 100060556@ku.ac.ae).

to complex and dynamic environments [1]. Soft robots possess flexible bodies that can bend, stretch, and deform. This flexibility proves particularly advantageous in scenarios requiring adaptability, dexterity, or interaction with delicate objects. However, the remarkable flexibility and infinite degrees of freedom inherent in soft robots pose significant challenges in modeling, controlling, or estimating their 3D morphology.

The significance of these robots has captured the attention of numerous researchers in recent decades, particularly concerning the advancement of mathematical models for the statics and dynamics of soft robots [2]. Despite numerous discoveries in modeling, the shape estimation of soft robots still requires further exploration. Estimation in soft robots is challenging, as it requires the development of efficient algorithms to extract valuable information from a large quantity of data recorded with camera system or embedded sensors.

The majority of existing works have focused on static estimation (or shape estimation), which assumes that the robot is in a quasi-static state. These works involve taking numerous discrete measurements along the continuum robot and then fitting a geometric model to these discrete measurements. For instance, [3] and [4] employ optimization methods to fit a given shape representation to discrete sensor data. The method in [3] employs curvature angle measurements with flex sensors, while [4] utilizes camera observations. However, these works utilize simplified geometric models that assume constant bending curvatures and only estimate the position and orientation of the robot's shape at certain points along its body, without taking into account internal strains. Other works on continuum robot state estimation are proposed in [5] using a filtering approach, or in the recent work [6], which uses Gaussian process regression together with a simple and general prior model allowing for efficient computations. Alternative approaches suggest extracting force information through shape sensing [7], [8] or simultaneously estimating the shape of continuum robots along with the applied forces [9], [10]. Moreover, [11] can predict the static deflection of cable-driven continuum robot using its length to correct the mechanical model to improve the control accuracy.

However, achieving full state estimation in soft robots, which encompasses not only the shape of the system but also its velocities, remains a challenge that only a few have successfully addressed. Theoretical studies on the convergence of these algorithms are hindered by the complexity of soft robot models. For example, in [12], an observer is proposed to estimate the full state of the system using the position and velocity of a few points along the robot's body. Similarly, [13] and [14] achieve full state estimation of soft robots from tip velocities. Nonetheless, the development of new algorithms capable of dynamically estimating system states holds significant promise for closing

the loop in control systems and enhancing the ability of soft robots.

This work focuses on developing a method for estimating the shape of slender soft robots, such as tentacles, using tendon-driven actuation for both actuation and shape estimation. Tendon-driven actuation is one of the prominent mechanisms in soft robotics [15]. It controls the motion of the soft body by retracting tendons embedded in the structure.

In this study, we introduce a dynamic algorithm capable of estimating the full state of slender soft robots using only the lengths and forces of the actuation tendons, assuming that the external forces are known. In their exact formulation, continuum soft robots belong to the domain of continuum mechanics, meaning their dynamics are governed by infinite-dimensional systems, typically represented by partial differential equations (PDEs). However, recent works have demonstrated that finite-dimensional approximations of these dynamics can be formulated using standard ordinary differential equations (ODEs).

For control or estimation purposes, the models often use a low-dimensional approximation that captures the essential dynamic behavior while possibly neglecting finer details [16]. In this direction, our approach is based on the recent GVS model [17], [18], which employs Cosserat rod theory and simplifies the model by using a finite set of strain bases. These strain bases capture the essential modes of deformation, allowing high-order modes truncation and resulting in simplified models that facilitate the design of estimation algorithms.

Using this truncation, we propose a linear state-space (SS) representation with state-dependent coefficients (SDC) where the inputs of the system are the actuator forces and the outputs are the actuator lengths. Additionally, a dynamic observer based on state-dependent Riccati equation (SDRE) is proposed to obtain the state dependent gain matrix that guarantees exponential stability of error estimation. SDRE observer is well-suited for nonlinear systems because it does not require linearization around an operating point. Instead, it uses a state-dependent model, which makes it more accurate for a wide range of operating conditions, showing its versatility and effectiveness, [19], [20].

The main distinction between our work and other methods in the literature investigating dynamic state estimation in slender soft robots lies in the sensors required for estimating the system's states. In our approach, only actuation readings are needed to estimate the full state of the system. This method efficiently integrates actuation and sensing into a compact form, eliminating the need for sensors along the robot's body or external camera observations. Previous works require the addition of extra sensors; for example, [12] necessitates a camera vision system to record the positions of several markers placed along the link, while [13] and [14] rely on an IMU sensor positioned at the tip of the soft robot. In the same direction of our work, [21], [22] use the intrinsic wrench of push-pull style continuum robots as a multi-axis force sensor to estimate both force and shape simultaneously; however, they consider the system at the equilibrium point, which differs significantly from the proposed work, where the shape is estimated dynamically. Other interesting works explore the possibility of shape sensing based on tendon length, as shown in [23], [24] and [25]. The main difference between these works and ours is that they require additional passive strings/tendons and the measurement of their lengths, whereas our work only measures the lengths of the actuated tendons. Measuring only the tendon lengths significantly increases the number of tendons required to estimate the shape, which
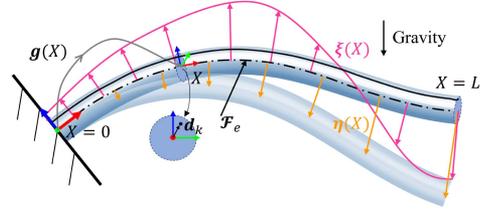
Fig. 1.   Schematic of GVS model.

can considerably complicate the design, especially when many tendons are embedded within the soft body. Moreover, while previous works primarily estimate states related to pose, our approach extends this by estimating states related to both pose and velocity. Our method operates under the assumption that external forces are known. Despite this limitation, it serves as an effective initial step with significant potential for practical applications.

II. GEOMETRIC VARIABLE STRAIN MODEL

In this section, we summarize the essential components of the Geometric Variable Strain (GVS) model used for simulating the dynamic response of a soft robot [26].

A. Kinematics

A slender soft manipulator can be modeled as a Cosserat rod, a continuous stack of rigid cross-sections parameterized by a curvilinear abscissa $X \in [0, L]$, where L is the length of the rod (Fig. 1). The homogeneous transformation matrix corresponding to a coordinate frame attached to these cross-sections is defined as the directed spatial curve $\boldsymbol{g}(\bullet) : X \to \boldsymbol{g}(X) \in SE(3)$:

$$\boldsymbol{g}(X,t) = \begin{bmatrix} \boldsymbol{R} & \boldsymbol{r} \\ \boldsymbol{0} & 1 \end{bmatrix}, \tag{1}$$

where $\boldsymbol{r}(X,t) \in \mathbb{R}^3$ is the position of the local frame, while $\boldsymbol{R}(X,t) \in SO(3)$ provides the orientation of the local frame relative to the spatial frame. Strain $\boldsymbol{\xi}$ and velocity $\boldsymbol{\eta}$ twists of the body are defined by the partial derivative of Equation (1) with respect to X $(\cdot)'$ and t $(\dot{\cdot})$:

$$\boldsymbol{g}'(X) = \boldsymbol{g}\hat{\boldsymbol{\xi}}, \quad \dot{\boldsymbol{g}}(X) = \boldsymbol{g}\hat{\boldsymbol{\eta}}, \tag{2}$$

where $(\hat{\bullet})$ indicates the isomorphism between $\mathbb{R}^6$ and $se(3)$. $\boldsymbol{\xi}$ and $\boldsymbol{\eta}$ are infinitesimal rigid transformations, that represent the rate of change of $\boldsymbol{g}$ in X and t.

The relation between screw strain and velocity is established through the equality of the mixed partial derivatives in space and time:

$$\boldsymbol{\eta}' = \dot{\boldsymbol{\xi}} - \mathrm{ad}_{\boldsymbol{\xi}}\boldsymbol{\eta} \tag{3}$$

where $\mathrm{ad}_{(\bullet)}$ is the adjoint operator of $se(3)$. Space integration of (2 a) and (3) provides:

$$\boldsymbol{g}(X) = \exp\left(\widehat{\boldsymbol{\Omega}}(X)\right), \tag{4}$$

$$\boldsymbol{\eta}(X) = \mathrm{Ad}_{\boldsymbol{g}^{-1}} \int_0^X \mathrm{Ad}_{\boldsymbol{g}}\dot{\boldsymbol{\xi}}ds \tag{5}$$

where $\mathrm{Ad}_{\boldsymbol{g}}$ is the adjoint representation of $\boldsymbol{g}$ and $\boldsymbol{\Omega}(X)$ is the Magnus expansion of $\boldsymbol{\xi}(X)$. The GVS approach employs a finite set of strain bases to discretize the continuous strain field. The states of the system are introduced as generalized coordinates that span the strain bases:

$$\boldsymbol{\xi}(X) = \boldsymbol{\Phi}_{\xi}(X)\boldsymbol{q} + \boldsymbol{\xi}^*(X) \tag{6}$$

where $\boldsymbol{\Phi}_{\xi}(X) \in \mathbb{R}^{6 \times n_{dof}}$ is the matrix function whose columns form the basis for the strain field, $\boldsymbol{q} \in \mathbb{R}^{n_{dof}}$, n_{dof} being the DoFs, is the vector of generalized coordinates for the chosen basis function and $\boldsymbol{\xi}^*$ is the reference strain computed at the stress-free state of the rod. Equation (6) can be substituted into (3), eventually leading to the definition of geometric Jacobian and its derivative:

$$\boldsymbol{\eta}(X) = \mathrm{Ad}_{\boldsymbol{g}(X)}^{-1} \int_0^X \mathrm{Ad}_{\boldsymbol{g}} \boldsymbol{\Phi}_{\xi} ds \dot{\boldsymbol{q}} = \boldsymbol{J}(\boldsymbol{q}, X)\dot{\boldsymbol{q}} \tag{7a}$$

$$\dot{\boldsymbol{\eta}}(X) = \boldsymbol{J}(\boldsymbol{q}, X)\ddot{\boldsymbol{q}} + \dot{\boldsymbol{J}}(\boldsymbol{q}, \dot{\boldsymbol{q}}, X)\dot{\boldsymbol{q}} \tag{7b}$$

Although (4) and (7) are analytical expressions, for a general variable strain case, they cannot be computed explicitly. However, a solution can be found through the recursive formulation of the kinematic equations, which employs a quadrature approximation of the Magnus expansion $\boldsymbol{\Omega}$, as detailed in [26].

B. Dynamics and Actuation

Projecting the free dynamics of the Cosserat rod [27] using the geometric Jacobian through D'Alembert's principle derives the generalized dynamics of the system in the standard Lagrangian form:

$$\boldsymbol{M}(\boldsymbol{q})\ddot{\boldsymbol{q}} + (\boldsymbol{C}(\boldsymbol{q}, \dot{\boldsymbol{q}}) + \boldsymbol{D})\dot{\boldsymbol{q}} + \boldsymbol{K}\boldsymbol{q} = \boldsymbol{B}_a(\boldsymbol{q})\boldsymbol{u}_a + \boldsymbol{F}(\boldsymbol{q}) , \tag{8}$$

where $\boldsymbol{M}(\boldsymbol{q}) \in \mathbb{R}^{n_{dof} \times n_{dof}}$, is the generalized mass matrix, $\boldsymbol{C}(\boldsymbol{q}, \dot{\boldsymbol{q}}) \in \mathbb{R}^{n_{dof} \times n_{dof}}$ is the Coriolis matrix, $\boldsymbol{D} \in \mathbb{R}^{n_{dof} \times n_{dof}}$ is the elastic damping matrix, $\boldsymbol{K} \in \mathbb{R}^{n_{dof} \times n_{dof}}$ is the stiffness matrix, $\boldsymbol{B}_a(\boldsymbol{q}) \in \mathbb{R}^{n_{dof} \times n_a}$ is the actuation matrix (n_a is the number of actuators), $\boldsymbol{F}(\boldsymbol{q}) \in \mathbb{R}^{n_{dof}}$ is the vector of generalized external forces, and $\boldsymbol{u}_a \in \mathbb{R}^{n_a}$ is the vector of applied actuation forces. Negative values of $\boldsymbol{u}_a$ indicate pulling forces, whereas positive values denote pushing forces. In the context of our study, $\boldsymbol{u}_a$ will be negative because tendon-driven actuators are capable only of producing pulling forces. $\boldsymbol{K}$ and $\boldsymbol{D}$ are computed based on Hooke-like linear elastic and viscoelastic constitutive laws, which is a reasonable approximation when the soft material is subjected to material strains that do not exceed 100% (see [28]). For more comprehensive details about the implementation of the different components of (8), readers may refer to [26].

For convenience, we express the external forces as inputs of our system, represented as $\boldsymbol{F}(\boldsymbol{q}) = \boldsymbol{B}_e(\boldsymbol{q})\boldsymbol{u}_e$, where $\boldsymbol{B}_e \in \mathbb{R}^{n_{dof} \times n_e}$ is the matrix of external force and $\boldsymbol{u}_e \in \mathbb{R}^{n_e}$ denotes the magnitude of the external forces. This allows us to combine actuation and external force using:

$$\boldsymbol{B}_a(\boldsymbol{q})\boldsymbol{u}_a + \boldsymbol{B}_e(\boldsymbol{q})\boldsymbol{u}_e = \boldsymbol{B}_\tau(\boldsymbol{q})\boldsymbol{u} , \tag{9}$$

where $\boldsymbol{u} = [\boldsymbol{u}_a^T, \boldsymbol{u}_e^T]^T$ and $\boldsymbol{B}_\tau(\boldsymbol{q}) = [\boldsymbol{B}_a(\boldsymbol{q}), \boldsymbol{B}_e(\boldsymbol{q})]$. Substituting (9) in (8) we get:

$$\boldsymbol{M}(\boldsymbol{q})\ddot{\boldsymbol{q}} + (\boldsymbol{C}(\boldsymbol{q}, \dot{\boldsymbol{q}}) + \boldsymbol{D}(\boldsymbol{q}))\dot{\boldsymbol{q}} + \boldsymbol{K}\boldsymbol{q} = \boldsymbol{B}_\tau(\boldsymbol{q})\boldsymbol{u} , \tag{10}$$

The generalized actuation force is obtained by projecting the actuation wrench acting on the rod's centerline [17]:

$$\boldsymbol{B}_a(\boldsymbol{q})\boldsymbol{u}_a = \int_0^L \boldsymbol{\Phi}_\xi^T \boldsymbol{\mathcal{F}}_a(X) dX, \tag{11a}$$

$$\boldsymbol{\mathcal{F}}_a(X) = \sum_{k=1}^{n_a} \begin{bmatrix} \tilde{\boldsymbol{d}}_k \boldsymbol{t}_k \\ \boldsymbol{t}_k \end{bmatrix} u_{a,k} = \boldsymbol{\Phi}_a(\boldsymbol{q}, X)\boldsymbol{u}_a, \tag{11b}$$

where $\boldsymbol{\Phi}_a(\boldsymbol{q}, X) \in \mathbb{R}^{6 \times n_a}$ is the actuation basis, $\boldsymbol{d}_k(X) = [0, \ p_{y,k}, \ p_{z,k}]^T$ is the cross-sectional position of actuator k, $\boldsymbol{t}_k(X)$ is the unit vector tangent to the actuator's path, and $\tilde{\bullet}$ is the skew-symmetric matrix representation of $so(3)$.

The kinematic equation relating the change in length of each actuator ($y_{a,k}$) with the state of the manipulator is given by [29],

$$\boldsymbol{y_a} = \boldsymbol{B}_a(\boldsymbol{q})^T \boldsymbol{q} + \boldsymbol{z_a}(\boldsymbol{q}) \tag{12}$$

where the kth component of $\boldsymbol{z_a}$ is given by,

$$z_{a,k}(\boldsymbol{q}) = \int_0^L (\boldsymbol{\Phi}_{a,k} - \boldsymbol{\Phi}_{a,k}{}^*)^T \left(\boldsymbol{\xi}^* - \begin{bmatrix} \boldsymbol{0} \\ \boldsymbol{d}_k' \end{bmatrix} \right) dX \tag{13}$$

and $\boldsymbol{\Phi}_{a,k}{}^*$ is the actuation basis of kth actuator when $\boldsymbol{\xi} = \boldsymbol{\xi}^*$.

Estimation problem: Given the soft robot model (10), the length of tendons $\boldsymbol{y_a}$, and the inputs of the system $\boldsymbol{u}$ (actuator and external forces), develop an algorithm to dynamically estimate the states of the soft robot.

III. SHAPE ESTIMATION PROBLEM

A. Formulation of the Estimation Problem

In this section, we formulate the nonlinear dynamics model (10) in a linear SS representation with SDC. This representation is necessary for developing the proposed dynamic observer, which aims to estimate the states of our system. We define the system's state vector as $\mathbf{x} = [\boldsymbol{q}, \dot{\boldsymbol{q}}]^T$. Then, from (10), we have:

$$\ddot{\boldsymbol{q}} = \boldsymbol{M}^{-1}(\boldsymbol{q}) \left(-(\boldsymbol{C}(\boldsymbol{q}, \dot{\boldsymbol{q}}) + \boldsymbol{D}(\boldsymbol{q}))\dot{\boldsymbol{q}} - \boldsymbol{K}\boldsymbol{q} + \boldsymbol{B}_\tau(\boldsymbol{q})\boldsymbol{u} \right) , \tag{14}$$

Combining (14) and (12), it yields

$$\begin{cases} \dot{\mathbf{x}} = \mathbf{A}(\mathbf{x})\mathbf{x} + \mathbf{B}(\mathbf{x})\mathbf{u}, \\ \mathbf{y} = \mathbf{C}(\mathbf{x})\mathbf{x} + \mathbf{z}(\mathbf{x}), \end{cases} \tag{15}$$

$$\mathbf{A}(\mathbf{x}) = \begin{pmatrix} \boldsymbol{0} & \mathbf{I} \\ -\boldsymbol{M}^{-1}\boldsymbol{K} & -\boldsymbol{M}^{-1}(\boldsymbol{C} + \boldsymbol{D}) \end{pmatrix},$$

$$\mathbf{B}(\mathbf{x}) = \begin{pmatrix} \boldsymbol{0} \\ \boldsymbol{M}^{-1}\boldsymbol{B}_\tau \end{pmatrix}, \ \mathbf{C}(\mathbf{x}) = [\boldsymbol{B}_a^T \ \boldsymbol{0}], \ \mathbf{z}(\mathbf{x}) = [\boldsymbol{z}_a^T \boldsymbol{0}]^T .$$

In the above SS representation $\mathbf{x} \in \mathbb{R}^n$ is the state, $\mathbf{u} \in \mathbb{R}^p$ is the input, and $\mathbf{y} \in \mathbb{R}^m$ is the output.

We make the following assumptions on the selected SDC form, which are necessary to demonstrate the local exponential stability of the proposed observer.

Assumption 1: The SDC parameterization $\mathbf{A}(\mathbf{x}), \mathbf{B}(\mathbf{x}), \mathbf{C}(\mathbf{x})$ and $\mathbf{z}(\mathbf{x})$ presented in (15) are at least locally Lipschitz.

Assumption 2: The time varying state-dependent matrix $\mathbf{C}(\mathbf{x})$ is bounded by $||\mathbf{C}(\mathbf{x})|| \leq \sigma_1$, where we denote the Euclidean norm as $|| \bullet ||$.

Assumption 3: Assume that the states and the input of the system are bounded by $||\mathbf{x}|| \leq \rho_1$ and $||\mathbf{u}|| \leq \rho_2$.

B. Differential State-Dependent Riccati Equation Observer

Consider the nonlinear continuous-time system represented by (15), then let us introduce an observer in the following manner:

$$\dot{\hat{\mathbf{x}}} = \mathbf{A}(\hat{\mathbf{x}})\hat{\mathbf{x}} + \mathbf{B}(\hat{\mathbf{x}})\mathbf{u} + \mathbf{K}(\hat{\mathbf{x}})(\mathbf{y} - \mathbf{C}(\hat{\mathbf{x}})\hat{\mathbf{x}} - \mathbf{z}(\hat{\mathbf{x}})), \quad (16)$$

where $\hat{\mathbf{x}}$ denotes the estimation of the states and $\mathbf{K}(\hat{\mathbf{x}})$ is the observer gain which is a varying $n \times m$ matrix. We define the observer gain as:

$$\mathbf{K}(\hat{\mathbf{x}}) = \mathbf{P}(\hat{\mathbf{x}})\mathbf{C}^{\mathbf{T}}(\hat{\mathbf{x}})\mathbf{R}^{-1}, \quad (17)$$

where $\mathbf{P}(\hat{\mathbf{x}}) \in \mathbb{R}^{n \times n}$ is a symmetric matrix which can be computed through the following state-dependent Riccati equation:

$$\mathbf{0} = (\mathbf{A}(\hat{\mathbf{x}}) + \alpha\mathbf{I})\mathbf{P}(\hat{\mathbf{x}}) + \mathbf{P}(\hat{\mathbf{x}})(\mathbf{A}^{\mathbf{T}}(\hat{\mathbf{x}}) + \alpha\mathbf{I})$$
$$- \mathbf{P}(\hat{\mathbf{x}})\mathbf{C}^{\mathbf{T}}(\hat{\mathbf{x}})\mathbf{R}^{-1}\mathbf{C}(\hat{\mathbf{x}})\mathbf{P}(\hat{\mathbf{x}}) + \mathbf{Q}. \quad (18)$$

where $\alpha > 0$ and $\mathbf{Q} \in \mathbb{R}^{n \times n}$ and $\mathbf{R} \in \mathbb{R}^{m \times m}$ are symmetric positive definite matrices. Note here that if we consider $\alpha = 0$, we obtain the usual state-dependent Riccati equation (SDRE). The scalar α is a design parameter which was proposed by [30] and indirectly indicates the error decay rate of the proposed exponential observer. We define the estimation error of the system as $\mathbf{e} = \mathbf{x} - \hat{\mathbf{x}}$, and subtracting (16) from (15), we obtain the error dynamics

$$\dot{\mathbf{e}} = \mathbf{A}(\mathbf{x})\mathbf{x} + \mathbf{B}(\mathbf{x})\mathbf{u} - \mathbf{A}(\hat{\mathbf{x}})\hat{\mathbf{x}} - \mathbf{B}(\hat{\mathbf{x}})\mathbf{u}$$
$$- \mathbf{K}(\hat{\mathbf{x}})(\mathbf{y} - \mathbf{C}(\hat{\mathbf{x}})\hat{\mathbf{x}} - \mathbf{z}(\hat{\mathbf{x}})). \quad (19)$$

Through manipulation and rearrangement of terms, the error dynamics can be written as follows:

$$\dot{\mathbf{e}} = [\mathbf{A}(\hat{\mathbf{x}}) - \mathbf{K}(\hat{\mathbf{x}})\mathbf{C}(\hat{\mathbf{x}})]\,\mathbf{e} + \boldsymbol{\beta}(\mathbf{x}, \hat{\mathbf{x}}, \mathbf{u}) - \mathbf{K}(\hat{\mathbf{x}})\boldsymbol{\lambda}(\mathbf{x}, \hat{\mathbf{x}})\,. \quad (20)$$

where

$$\boldsymbol{\beta}(\mathbf{x}, \hat{\mathbf{x}}, \mathbf{u}) = [\mathbf{A}(\mathbf{x}) - \mathbf{A}(\hat{\mathbf{x}})]\,\mathbf{x} + [\mathbf{B}(\mathbf{x}) - \mathbf{B}(\hat{\mathbf{x}})]\,\mathbf{u}$$
$$\boldsymbol{\lambda}(\mathbf{x}, \hat{\mathbf{x}}) = [\mathbf{C}(\mathbf{x}) - \mathbf{C}(\hat{\mathbf{x}})]\,\mathbf{x} + [\mathbf{z}(\mathbf{x}) - \mathbf{z}(\hat{\mathbf{x}})]\,.$$

Theorem 1 of [30] demonstrates that the error dynamics (20) is locally exponentially stable around the equilibrium point $\mathbf{e} = \mathbf{0}$, provided that Assumptions 1–3 hold and the solution $\mathbf{P}(\hat{\mathbf{x}})$ of the differential Riccati (18) is bounded for some positive real numbers. Verifying condition (18) for our nonlinear system requires solving the equation iteratively over time, computing $\mathbf{P}(\hat{\mathbf{x}})$, and updating the observer gain $\mathbf{K}(\hat{\mathbf{x}})$.

Remark 1: The Lipschitz conditions outlined in Assumption 1 are also considered in [30] and in prior research on SDRE observers. The additional restrictive assumption regarding the SDC form in our work is that $\mathbf{z}(\mathbf{x})$ must be locally Lipschitz. The function $\mathbf{z}(\mathbf{x})$ is continuous, smooth, and bounded. Thus, there exists a constant $\kappa_1 > 0$ such that

$$||\mathbf{z}(\mathbf{x_1}) - \mathbf{z}(\mathbf{x_2})|| \le \kappa_1||\mathbf{x_1} - \mathbf{x_2}||.$$

for $\mathbf{x_1}, \mathbf{x_2} \in \mathbb{R}^n$. Then, we can observe that the magnitude of $\boldsymbol{\lambda}(\mathbf{x}, \hat{\mathbf{x}})$ still remains bounded, which is necessary for demonstrating Theorem 1 of [30].

$$||\boldsymbol{\lambda}(\mathbf{x}, \hat{\mathbf{x}})|| = ||\,[\mathbf{C}(\hat{\mathbf{x}}) - \mathbf{C}(\mathbf{x})]\,\mathbf{x}|| + ||\mathbf{z}(\hat{\mathbf{x}}) - \mathbf{z}(\mathbf{x})||$$
$$\le \kappa_2||\mathbf{x} - \hat{\mathbf{x}}||.$$

TABLE I
ACTUATOR ROUTING: $r(X) = r_b - (r_b - R_t)X$

Number	Actuator range (m)	z-Coordinate (m)	y-Coordinate (m)
1	$[0, L]$	$r(X)$	0
2	$[0, L]$	$-r(X)\sin(\pi/6)$	$-r(X)\cos(\pi/6)$
3	$[0, L]$	$-r(X)\sin(\pi/6)$	$r(X)\cos(\pi/6)$

where $\kappa_2 > 0$ is a real number. Then, the key condition for assuring the estimation error convergence is closely related with the existence of positive bounds of the solution of $\mathbf{P}(\hat{\mathbf{x}})$ of the state-dependent Riccati (18). These results imply that the pair $(\mathbf{C}, \mathbf{A} + \alpha\mathbf{I})$ has to be pointwise observable in the linear sense for all $\mathbf{x}$ in the domain of interest. This observability condition can be checked by the Popov-Belevitch-Hautus test:

$$rank\left(\begin{bmatrix} \lambda\mathbf{I} - (\mathbf{A} + \alpha\boldsymbol{I}) \\ \mathbf{C} \end{bmatrix}\right) = n; \quad \forall\,\lambda \in \mathbb{C}, \quad (21)$$

The sensors needed to ensure the system's observability must supply independent vectors to address the rank deficiency.

IV. SIMULATION RESULTS

To assess the efficacy of the proposed estimation technique, we conducted numerical simulations employing different Legendre polynomial bases for each of the six strain fields of the Cosserat rod. Within the simulations, we calculated the lengths of the tendons using the kinematic formula (12) and we implement the proposed observer (16), with parameters set as follows: $\boldsymbol{Q} = 10\boldsymbol{I}_{n \times n}$, $\boldsymbol{R} = 0.1\boldsymbol{I}_{m \times m}$ and $\alpha = 1$. We conducted simulations on a 0.25 m-long soft manipulator featuring a Young modulus of 2 MPa, a density of 1121 kg/m³, a Poisson ratio of 0.5, and an elastic damping factor of 5 kPa. The radius of the manipulator, $r(X)$, linearly decreases from a base radius, r_b, of 12.5 mm to a tip radius, r_t, of 3 mm. The routing parameters of the tendons are specified in Table I.

The bases of our system are defined using Legendre polynomial bases, where $\mathcal{L}_i(X)$ denotes a Legendre polynomial of order i. A polynomial of degree i contributes $i + 1$ DoF, giving a total DoF of the robot as the sum across all six fields. Legendre polynomials are well-suited as basis functions for strain fields in due to their orthogonality over a finite interval. Consequently, an example of using Legendre polynomial bases in the strain field (6) is shown as follows:

$$\boldsymbol{\Phi}_\xi = \begin{bmatrix} \mathcal{L}_0(X) & 0 & 0 & 0 & 0 \\ 0 & \mathcal{L}_0(X) & 0 & 0 & 0 \\ 0 & 0 & \mathcal{L}_0(X) & \mathcal{L}_1(X) & \mathcal{L}_2(X) \\ 0 & 0 & 0 & 0 & 0 \\ 0 & 0 & 0 & 0 & 0 \\ 0 & 0 & 0 & 0 & 0 \end{bmatrix} \quad (22)$$

where torsion is represented by the first Legendre polynomial, bending about the y-axis is represented by the first Legendre polynomial and bending about the z-axis is represented by the first three Legendre polynomials. This basis matrix allow us to employ different orders of polynomial for each strain. Finally, the system dynamics and the equation of the observer are solved using explicit numerical integrators implemented by ode45 MATLAB functions.
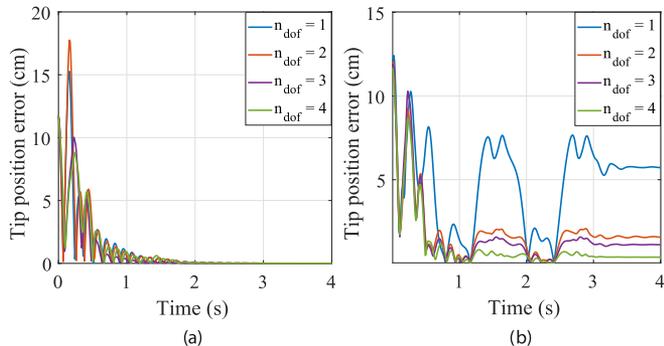
Fig. 2. Tip position estimation error using 1 actuator. (a) The same model dimension was used for both the dynamic model and the algorithm implementation. (b) We implement our algorithm in a high model dimension model.

TABLE II
COMPUTATIONAL TIME AND AVERAGE POSITION MISMATCH

Basis Type	n_{dof}	Time (s)	t_r	Error (cm)
Legendre	1	1.02	0.26	5.16
Legendre	2	3.65	0.91	1.89
Legendre	3	17.30	4.33	1.58
Legendre	4	21.21	5.30	1.07

t_r represents the ratio between the computational time and the real-time duration.

A. One Tendon

In the first two sets of simulations, the manipulator is equipped with the first linear actuator of Table I. We actuate the system with a sinusoidal input of frequency $\omega = 5$ rad/s and amplitude of $A_s = 7$ N during 4s, including only gravity as the external force. We tested the proposed estimation method by employing Legendre polynomials bases. Four cases have been considered here: 1) constant curvature, $n_{dof} = 1$, 2) linear curvature $n_{dof} = 2$, 3) linear curvature and constant elongation $n_{dof} = 3$ and 3) quadratic curvature and constant elongation $n_{dof} = 4$. Even in this case, where the system has only one tendon and is deformed in 2D, we test polynomials with different numbers of DoF to capture the deformation considering both internal actuation and external forces. The importance of using more DoF for complex deformations has been demonstrated in previous works, such as [18], [31].

In these simulations, the bases used for the dynamic simulation of the soft manipulator and those employed to implement the estimation algorithm are the same. The results indicate excellent convergence of the estimated shape to the real one across all four cases. Fig. 2(a) shows the error at the tip for all the cases. Moreover, the results illustrate that the estimation error converges exponentially to zero within a timeframe of less than 2 seconds. Condition (21) was verified for the four cases.

Additionally, tests were conducted using the proposed observer in a higher-dimensional model to evaluate its performance when employing a limited number of DoF in more complex models. A Legendre polynomial of 4th order was utilized for both curvature and elongation for the dynamic simulation, resulting in a total of 10 DoF. Fig. 2(b) illustrates the error at the tip position for the four cases, while Table II presents the computational time and the average error at the tip. The time listed in the table represents the total computation time required to execute the estimation algorithm for the entire simulation

in a single batch, using a sampling rate of 100 Hz. While the estimation error converges to a close region of the solution, there is a noticeable error due to the disparity between the degrees of freedom used in the simulation and those employed in the observer. As we increase the number of degrees of freedom in the observer, the accuracy improves, as the model captures more of the system's dynamics, though at the cost of increased computational complexity.

Increasing the system's degrees of freedom amplifies the computational load due to the larger system matrices. Moreover, the necessity to solve (18) at each iteration further contributes to the computational burden. Note that for the two first cases the implementation of the observer is faster than real time using a sampling rate of 100 Hz. This indicates that the average computational speed for both the first and second-order computations exceeds 100 Hz. We attempted to utilize higher-order Legendre polynomials, but unfortunately, the solution for (18) does not exist and the condition (21) is not satisfied. This highlights that only one measurement is insufficient for observing system states if the number of DoF is high. One potential solution to increase the number of degrees of freedom that we can observe is to increase the number of independent measurements in our system, which involves adding more tendons. This augmentation would provide more information about the shape of the soft robots as we will explore in the next section.

B. Three Tendons

In this section, we simulate the manipulator with the same properties but with the three linear actuators of Table I. We simulate the proposed estimation method by using explicit quadratic Legendre polynomial in both curvature (y, z) and constant elongation $n_{dof} = 7$.

We actuate the system in order to perform a circle trajectory with the tip with an angular frequency of $\omega = 5$ rad/s and amplitude of $A_s = 7$ N during 5s. We test the proposed estimation method in two cases: 1) only gravity is included as the external force and 2) gravity and a point force $\mathcal{F}_e = [0, 0, 0, 0, 0, -1.5]^T$ N in the middle of the rod are included as the external forces. Also, we have added a step disturbance force at the tip between 2 s and 2.25 s. Fig. 3 shows that even with significant intentional deviations in the initial state estimation from the true value, our methodology swiftly converges towards the actual shape and accurately tracks the system's states thereafter in both cases. Note that the temporary disturbance creates a deviation between the current states and the estimated ones while it is present, having the same effect as starting with an initial guess that differs from the actual state once the disturbance is gone. Moreover, Fig. 3(b) illustrates the convergence of certain states $(q, \dot{q})$ of the system for Case 1). These results show that our estimation method can accommodate a higher number of DoF due to the increased number of independent measurements (3 tendons actuators), thereby enhancing the observability of our system.

Finally, we intentionally chose an initial estimation $\hat{x}_0$ that is significantly different from the initial state x_0 to emphasize a key aspect of the observer's development: even when the initial estimate differs greatly from the actual initial state, the estimation still converges to the correct solution.

V. EXPERIMENTAL VERIFICATION

The performance of the proposed estimation method is assessed in a experimental prototype in order to demonstrate the
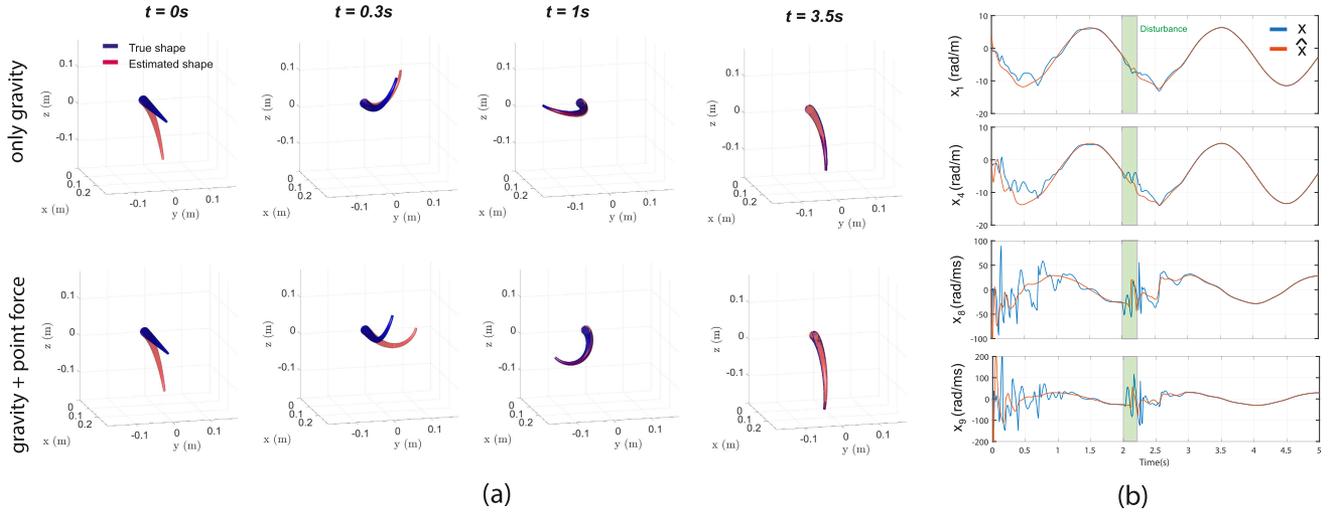
Fig. 3. Three tendons estimation. (a) True and estimated shape. (b) Convergence of some estimated states (pose and velocities).

validity of our approach in real scenarios. The actuation of the tendon is driven by the rotation of a pulley which is connected to the end of the tendon and generate the pulling movements to actuate the system. The length variation of the tendons is measured through the rotation of the pulley using a magnetic encoder, while the actuator force (negative of tendon tension) is measured using a highly accurate Micro S-type Load Cell B313-20N with a precision of $\pm\, 0.05\%$ F.S. placed between the pulley and the tendon. To capture the position of the manipulator tip, we utilize the `Motive` motion capture camera system (Optitrack Prime^X 22). The tracking system, having a total of 24 high-speed infrared cameras, provides ultra-low latency tracking at a sampling speed of 90 Hz. In the experiments, we actuate the system with the actuator 1 of Table I. We deliberately chose this simplified case over the more complex 3D scenario to maintain clarity in the analysis. This allows us to assess the efficacy of our algorithm while avoiding additional sources of error that more complex experimental conditions might introduce.

A. Discrete Disk Actuation With Friction

In our experiment, we used a soft robot prototype where the tendon actuators are routed externally through disk-guides. Since the contact with the disks involves friction, accurate modeling of tension loss at the contact points is crucial. We use the Capstan equation to quantify this frictional effect [32]:

$$\frac{u_{a,i+1}}{u_{a,i}} = e^{-\mu\phi_i}; \qquad \phi_i = \cos^{-1}\left(-\boldsymbol{v}_{L_i}^T \boldsymbol{v}_{R_i}\right) \qquad (23)$$

μ is the coefficient of friction, i is the disk index, and $\boldsymbol{v}_L, \boldsymbol{v}_R$ are unit vectors in the actuator directions on both sides of the guiding disk (see Fig. 4). The subscript k of actuators is intentionally dropped here since only one tendon is used in the experiment. The resultant actuation force $\boldsymbol{f}_i$, expressed in the local frame of the robot, is given by:

$$\boldsymbol{f}_i = \boldsymbol{v}_{L_i} u_{a,i} + \boldsymbol{v}_{R_i} u_{a,i+1}, \qquad (24)$$

which can then be considered as a concentrated force at the contact point.
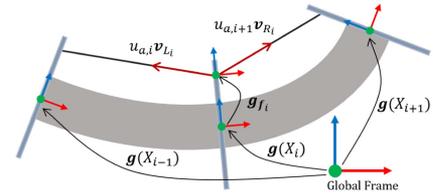
Fig. 4. Externally disk-guided actuation model.
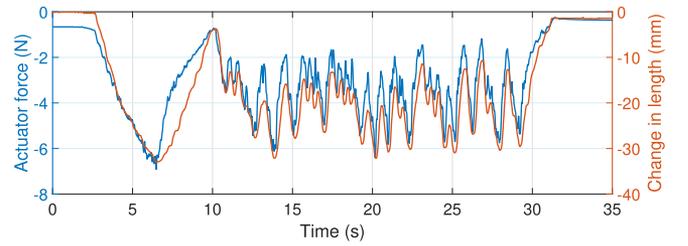
Fig. 5. Actuator force and length variation.
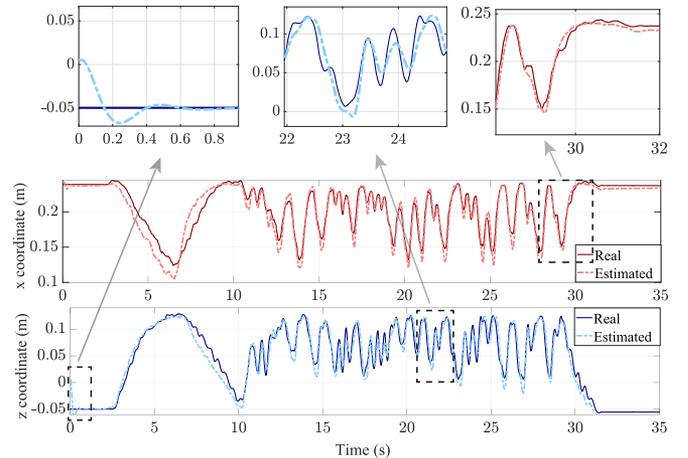
Fig. 6. Comparison between the real and estimated tip position.
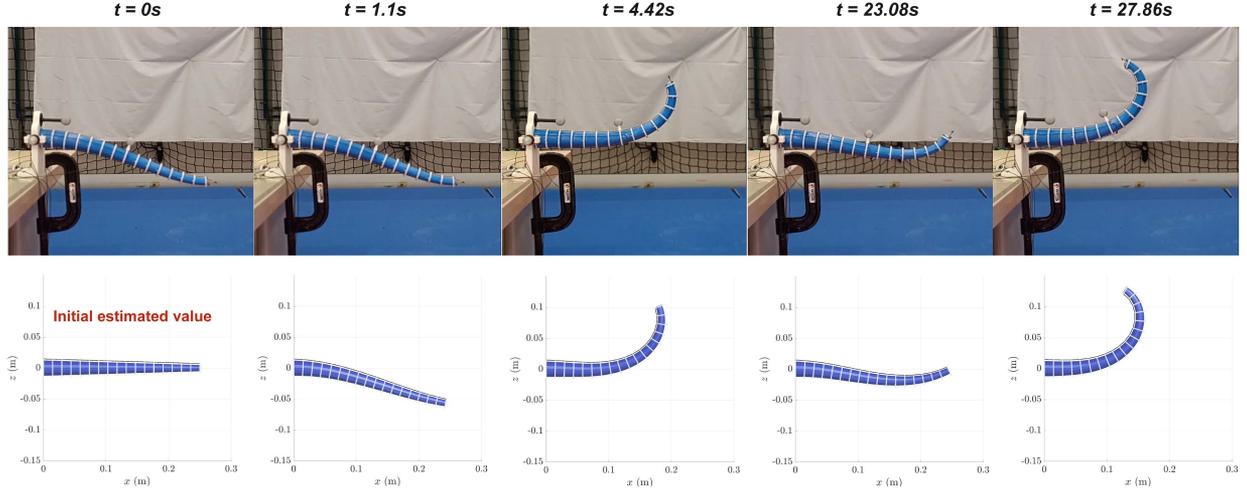
Fig. 7.   Comparison of the true shape and estimated shape using the experimental prototype.

Using (23) and (24), we compute the point wrench on the manipulator's centerline at the disk's location:

$$\mathcal{F}(X_i) = \mathrm{Ad}^*_{g_{f_i}} \begin{bmatrix} \mathbf{0} \\ \mathbf{v}_{L_i} + \mathbf{v}_{R_i} e^{-\mu \phi_i} \end{bmatrix} e^{-\mu \sum_{j=1}^{i-1} \phi_j} u_a \quad (25)$$

while the generalized actuation force is given by,

$$\boldsymbol{B}_a \boldsymbol{u}_a = \sum_{i=1}^{n_d} \boldsymbol{J}(X_i)^T \mathcal{F}(X_i) \quad (26)$$

where n_d is the number of guiding disks and $\boldsymbol{g}_{f_i}$ is the transformation matrix from the central line of the manipulator to the contact point.

B. Experimental Results

We implemented the proposed estimation approach outlined in (16)–(18) in our prototype. Material properties for the prototype were identified experimentally, yielding a Young's modulus of 2 MPa, a density of 1121 kg/m^3, a tendon friction coefficient of 0.1 (μ in (25)) and a elastic damping coefficient of 3.3 kPas. To achieve this, we divided the process into several steps. First, the properties of the link (equivalent density and Young Modulus) are estimated by placing various weights at the tip without actuating the system. We then seek optimal parameters to minimize the difference between the real measured marker positions and those obtained when the model is in equilibrium: $\boldsymbol{Kq} = \boldsymbol{B}_a(\boldsymbol{q})\boldsymbol{u}_a + \boldsymbol{F}(\boldsymbol{q})$. Once these properties are determined, the tendon friction is calibrated by applying different tensions to the tendons and minimizing again the real measured marker positions and that obtained when the model is in equilibrium. The proposed identification method is based on the measurement of the three markers located at the midpoint, three-quarters point, and the tip of the manipulator in N sets of different experiments. A similar approach was presented in [33] to identify the parameters of the model. Finally, the elastic damping coefficient was estimated by recording the system's response to an initial force applied at the tip and matching this response with the model's predicted behavior. Based on the results obtained from the simulation section, we have selected the Legendre polynomials with linear curvature and constant elongation ($n_{dof} = 3$).

This is a good compromise between computational load and the accuracy achieved in fitting our model. We conducted random actuation for 35 s. The actuation readings used for estimating the states and the estimation results are illustrated in Figs. 5 and 6, respectively.

Fig. 6 also shows zoomed-in views of three different parts of the experiments: 1) the initial guess phase, where the system converges in 0.3 seconds, 2) the middle of the experiment to highlight the estimation during dynamic changes, particularly where the velocity direction changes and 3) the end of the experiment to demonstrate how the observer converges at the conclusion of the experiment. The average tip position error in the experiment is 1.79 cm, approximately 7% of the length of the actuator. The error at the tip of the robot is computed as the norm of the distance between the estimated tip position and the tip position measured by our camera system. The estimated tip position is determined by recursively evaluating (4) until the tip. This is done for each iteration where the generalized coordinates $\boldsymbol{q}$ are updated using our estimation algorithm.

VI. CONCLUSION

This study introduces an innovative estimation technique capable of dynamically observing the states of slender soft manipulators, including pose and velocity, solely through the actuator forces and length of their tendons. Unlike other methods, this approach exclusively utilizes actuation readings, without the need for supplementary sensory systems such as cameras or embedded sensors. Combining the GVS approach with a kinematic formula for actuator length variation and a nonlinear observer design SDRE, we investigate the potential of this new method. The GVS approach enables us to approximate the infinite DoF nature of soft robots by employing a finite set of strain bases, which can be expressed in a 'bunch' of DoFs. However, increasing the DoFs of the system significantly raises computational time and may compromise the existence of a bounded, positive solution of the Riccati (18), crucial for ensuring stability in the error dynamics. Through simulations and experimental validation, we test the efficiency of our method across various DoFs and actuator numbers, employing Legendre

polynomial strain bases. The SDRE observer shows good convergence properties in the complex nonlinear system considered in this work; however, its efficiency is highly dependent on the accuracy of the state-dependent model. Future research will focus on exploring optimal strain bases through data-driven methods to reduce DoFs, resulting in a more precise model with reduced computational time, a crucial consideration for real-time applications. In addition, the proposed approach relies heavily on the assumption that external forces are known. There are numerous scenarios where this technique can be effectively applied, such as in free-contact movements for inspection tasks utilizing a camera at the tip, or in pick-and-place operations where the mass of the objects is predetermined. We envision enhancing this approach with complementary sensors to estimate external forces, enabling its application in more complex scenarios.

REFERENCES

[1] C. Laschi, B. Mazzolai, and M. Cianchetti, "Soft robotics: Technologies and systems pushing the boundaries of robot abilities," *Sci. Robot.*, vol. 1, no. 1, 2016, Art. no. eaah3690.

[2] C. Armanini, F. Boyer, A. T. Mathew, C. Duriez, and F. Renda, "Soft robots modeling: A structured overview," *IEEE Trans. Robot.*, vol. 39, no. 3, pp. 1728–1748, Jun. 2023.

[3] J. Y. Loo, K. C. Kong, C. P. Tan, and S. G. Nurzaman, "Non-linear system identification and state estimation in a pneumatic based soft continuum robot," in *2019 IEEE Conf. Control Technol. Appl.*, 2019, pp. 39–46.

[4] Y. Chen et al., "Model-based estimation of the gravity-loaded shape and scene depth for a slim 3-actuator continuum robot with monocular visual feedback," in *Proc. 2019 Int. Conf. Robot. Automat.*, 2019, pp. 4416–4421.

[5] P. L. Anderson, A. W. Mahoney, and R. J. Webster, "Continuum reconfigurable parallel robots for surgery: Shape sensing and state estimation with uncertainty," *IEEE Robot. Automat. Lett.*, vol. 2, no. 3, pp. 1617–1624, Jul. 2017.

[6] S. Lilge, T. D. Barfoot, and J. Burgner-Kahrs, "Continuum robot state estimation using Gaussian process regression on se (3)," *Int. J. Robot. Res.*, vol. 41, no. 13/14, pp. 1099–1120, 2022.

[7] Q. Qiao, G. Borghesan, J. De Schutter, and E. V. Poorten, "Force from shape—estimating the location and magnitude of the external force on flexible instruments," *IEEE Trans. Robot.*, vol. 37, no. 5, pp. 1826–1833, Oct. 2021.

[8] C. Della Santina, R. L. Truby, and D. Rus, "Data–driven disturbance observers for estimating external forces on soft robots," *IEEE Robot. Automat. Lett.*, vol. 5, no. 4, pp. 5717–5724, Oct. 2020.

[9] J. M. Ferguson, D. C. Rucker, and R. J. Webster, "Unified shape and external load state estimation for continuum robots," *IEEE Trans. Robot.*, vol. 40, pp. 1813–1827, 2024.

[10] A. Y. Alkayas, D. Feliu-Talegon, A. T. Mathew, C. Rucker, and F. Renda, "Shape and tip force estimation of concentric tube robots based on actuation readings alone," in *Proc. 2023 IEEE Int. Conf. Soft Robot.*, 2023, pp. 1–8.

[11] X. Wei, F. Ju, H. Guo, B. Chen, and H. Wu, "Modeling and control of cable-driven continuum robot used for minimally invasive surgery," *Proc. Inst. Mech. Eng., Part H, J. Eng. Med.*, vol. 237, no. 1, pp. 35–48, 2023.

[12] C. Rucker, E. J. Barth, J. Gaston, and J. C. Gallentine, "Task-space control of continuum robots using underactuated discrete rod models," in *2022 IEEE/RSJ Int. Conf. Intell. Robots Syst.*, 2022, pp. 10967–10974.

[13] K. Stewart, Z. Qiao, and W. Zhang, "State estimation and control with a robust extended Kalman filter for a fabric soft robot," *IFAC-PapersOnLine*, vol. 55, no. 37, pp. 25–30, 2022.

[14] T. Zheng, Q. Han, and H. Lin, "Full state estimation of continuum robots from tip velocities: A cosserat-theoretic boundary observer," *IEEE Trans. Automa. Control*, 2024, doi: 10.1109/TAC.2024.3485404.

[15] S. Zaidi, M. Maselli, C. Laschi, and M. Cianchetti, "Actuation technologies for soft robot grippers and manipulators: A review," *Curr. Robot. Rep.*, vol. 2, no. 3, pp. 355–369, 2021.

[16] C. Della Santina, C. Duriez, and D. Rus, "Model-based control of soft robots: A survey of the state of the art and open challenges," *IEEE Control Syst. Mag.*, vol. 43, no. 3, pp. 30–65, Jun. 2023.

[17] F. Renda, C. Armanini, V. Lebastard, F. Candelier, and F. Boyer, "A geometric variable-strain approach for static modeling of soft manipulators with tendon and fluidic actuation," *IEEE Robot. Automat. Lett.*, vol. 5, no. 3, pp. 4006–4013, Jul. 2020.

[18] F. Boyer, V. Lebastard, F. Candelier, and F. Renda, "Dynamics of continuum and soft robots: A strain parameterization based approach," *IEEE Trans. Robot.*, vol. 37, no. 3, pp. 847–863, Jun. 2021.

[19] S. R. Nekoo, "Tutorial and review on the state-dependent Riccati equation," *J. Appl. Nonlinear Dyn.*, vol. 8, no. 2, pp. 109–166, 2019.

[20] T. Çimen, "State-dependent Riccati equation (SDRE) control: A survey," *IFAC Proc. Volumes*, vol. 41, no. 2, pp. 3761–3775, 2008.

[21] K. Xu and N. Simaan, "An investigation of the intrinsic force sensing capabilities of continuum robots," *IEEE Trans. Robot.*, vol. 24, no. 3, pp. 576–587, Jun. 2008.

[22] K. Xu and N. Simaan, "Intrinsic wrench estimation and its performance index for multisegment continuum robots," *IEEE Trans. Robot.*, vol. 26, no. 3, pp. 555–561, Jun. 2010.

[23] W. S. Rone and P. Ben-Tzvi, "Multi-segment continuum robot shape estimation using passive cable displacement," in *Proc. 2013 IEEE Int. Symp. Robot. Sensors Environ.*, 2013, pp. 37–42.

[24] A. L. Orekhov, E. Z. Ahronovich, and N. Simaan, "Lie group formulation and sensitivity analysis for shape sensing of variable curvature continuum robots with general string encoder routing," *IEEE Trans. Robot.*, vol. 39, no. 3, pp. 2308–2324, Jun. 2023.

[25] J. Li, F. Zhang, Z. Yang, Z. Jiang, Z. Wang, and H. Liu, "Shape sensing for continuum robots by capturing passive tendon displacements with image sensors," *IEEE Robot. Automat. Lett.*, vol. 7, no. 2, pp. 3130–3137, Apr. 2022.

[26] A. T. Mathew, D. Feliu-Talegon, A. Y. Alkayas, F. Boyer, and F. Renda, "Reduced order modeling of hybrid soft-rigid robots using global, local, and state-dependent strain parameterization," *Int. J. Robot. Res.*, pp. 1–26, 2024, doi: 10.1177/02783649241262.

[27] F. Boyer and F. Renda, "Poincare's equations for cosserat media: Application to shells," *J. Nonlinear Sci.*, vol. 27, no. 1, pp. 1–44, 2017.

[28] A. T. Mathew, I. M. B. Hmida, C. Armanini, F. Boyer, and F. Renda, "Sorosim: A MATLAB toolbox for hybrid rigid-soft robots based on the geometric variable-strain approach," *IEEE Robot. Automat. Mag.*, vol. 30, no. 3, pp. 106–122, Sep. 2023.

[29] F. Renda, C. Armanini, A. Mathew, and F. Boyer, "Geometrically-exact inverse kinematic control of soft manipulators with general threadlike actuators' routing," *IEEE Robot. Automat. Lett.*, vol. 7, no. 3, pp. 7311–7318, Jul. 2022.

[30] H. Beikzadeh and H. D. Taghirad, "Exponential nonlinear observer based on the differential state-dependent Riccati equation," *Int. J. Automat. Comput.*, vol. 9, pp. 358–368, 2012.

[31] F. Stella, Q. Guan, C. Della Santina, and J. Hughes, "Piecewise affine curvature model: A reduced-order model for soft robot-environment interaction beyond PCC," in *Proc. 2023 IEEE Int. Conf. Soft Robot.*, 2023, pp. 1–7.

[32] W. S. Rone and P. Ben-Tzvi, "Continuum robot dynamics utilizing the principle of virtual power," *IEEE Trans. Robot.*, vol. 30, no. 1, pp. 275–287, Feb. 2014. [Online]. Available: https://ieeexplore.ieee.org/document/6613525/

[33] H. Li, L. Xun, and G. Zheng, "Piecewise linear strain Cosserat model for soft slender manipulator," *IEEE Trans. Robot.*, vol. 39, no. 3, pp. 2342–2359, Jun. 2023.